
Neuropathic Pain Diagnosis Simulator for Causal Discovery Algorithm Evaluation

Ruibo Tu

KTH Royal Institute of Technology
ruibo@kth.se

Kun Zhang

Carnegie Mellon University
kunz1@cmu.edu

Bo Christer Bertilsson

Karolinska Institute
bo.bertilsson@ki.se

Hedvig Kjellström

KTH Royal Institute of Technology
hedvig@kth.se

Cheng Zhang

Microsoft Research, Cambridge
Cheng.Zhang@microsoft.com

Abstract

Discovery of causal relations from observational data is essential for many disciplines of science and real-world applications. However, unlike other machine learning algorithms, whose development has been greatly fostered by a large amount of available benchmark datasets, causal discovery algorithms are notoriously difficult to be systematically evaluated because few datasets with known ground-truth causal relations are available. In this work, we handle the problem of evaluating causal discovery algorithms by building a flexible simulator in the medical setting. We develop a neuropathic pain diagnosis simulator, inspired by the fact that the biological processes of neuropathic pathophysiology are well studied with well-understood causal influences. Our simulator exploits the causal graph of the neuropathic pain pathology and its parameters in the generator are estimated from real-life patient cases. We show that the data generated from our simulator have similar statistics as real-world data. As a clear advantage, the simulator can produce infinite samples without jeopardizing the privacy of real-world patients. Our simulator provides a natural tool for evaluating various types of causal discovery algorithms, including those to deal with practical issues in causal discovery, such as unknown confounders, selection bias, and missing data. Using our simulator, we have evaluated extensively causal discovery algorithms under various settings.

1 Introduction

Many real-life decision-making processes require an understanding of underlying causal relations. For example, understanding the cause of symptoms is essential for physicians to make correct treatment decisions; understanding the cause of observed environmental changes is critical to take action against global warming. However, it is generally infeasible or even impossible to do interventions or randomized experiments to verify these causal relations. Therefore, causal discovery from observational data has attracted much attention [29, 31, 40, 49].

However, the evaluation of causal discovery algorithms has been a challenge [3]. The great application demand also indicates that ground-truth causal relations in a complex scenario are often unknown to humans. The lack of systematic evaluations of causal discovery algorithms has hindered both the development of the field and the impact of these algorithms on solving real-life problems. Research-wise, it is hard to identify the advantages and disadvantages of causal discovery algorithms performing in real-world scenarios. A systematic way to evaluate causal discovery algorithms is pressing.

Other machine learning disciplines such as supervised learning and reinforcement learning have made great success in real-world applications such as image classification [34, 45] and speech recognition [2]. An important driving factor for their fast development and great success is the existence of a large amount of benchmark datasets for systematic evaluation. The benchmark datasets can be in the form of large-scale labeled and publicly available datasets such as [13, 22], which are commonly used for supervised and unsupervised learning. They can also be in the form of synthetic data that are generated from simulators, e.g. an autonomous driving simulator [4], an agent motion [5], and a gaming environment [19]. Such simulators accelerate the development of reinforcement learning algorithms and promote usage in real-life applications.

Establishing benchmark datasets for the evaluation of causal discovery algorithms will naturally accelerate the development of this research discipline and increase its real-world impact. However, it is difficult to collect such datasets with known ground-truth because underlying real-world causal relations are usually highly complex. Fortunately, domain experts in disciplines such as biology and physics can provide information about well-understood causal influences in some specific scenarios. This gives us opportunities to utilize domain knowledge to reveal ground-truth causal relations and build realistic simulators. In this way, we can generate data from simulators and use such benchmark datasets for the evaluation of causal discovery algorithms.

In this work, we present a neuropathic pain diagnosis simulator for evaluating causal discovery algorithms. As one of the most important healthcare issues, neuropathic pain is well-studied in bio-medicine and has well-understood causal influences. By definition, neuropathic pain is caused by disease or injury of the nervous system. It includes various chronic conditions that, together, affect up to 8% of the population. The prevalence of neuropathic pain increased to 60% in those with severe clinical neuropathy [9]. We build a simulator based on the causal relations in neuropathic pain diagnoses. Given the causal relations, we estimate the parameters of the corresponding causal graph using a small cohort of anonymous real-world clinical records to generate simulated data. Our simulator not only provides the simulated data and the ground-truth causal relations for evaluating causal discovery algorithms but also builds up a bridge between machine learning and neuropathic pain diagnoses. In summary, our contribution is a neuropathic pain diagnosis simulator. Especially:

- It represents a complex real-world scenario with more than 200 variables and around 800 well-defined causal relations. It can also generate any amount of data without jeopardizing security or privacy of patients' data (Section 2).
- Our simulator can produce data indistinguishable from real-world data. We have verified the simulation quality using both medical expertise and statistical evaluation (Section 3).
- Our simulator is flexible and can be used to generate data with different practical issues, such as confounding, selection bias, and missing data (Section 2.3 and Section 4).
- We have evaluated major causal discovery algorithms, including PC [40], FCI [40], and GES [6] with simulated data under different settings (Section 4).

2 Neuropathic Pain Simulator

In this section, we introduce our neuropathic pain diagnosis simulator ¹. We first show essential causal relations in the neuropathic pain diagnosis, and then present details of the simulator design. Finally, we discuss some open problems in causal discovery and how to use our simulator to simulate instances of such problems.

2.1 Causal Relations for Neuropathic Pain Diagnosis

Neuropathic pain diagnoses mainly contain symptom diagnosis, pattern diagnosis, and pathophysiological diagnosis. For example, Table 1a shows typical neuropathic pain diagnostic records. *Symptom diagnosis* describes the discomfort of patients. *Pattern diagnosis* identifies symptom patterns. In neuropathic pain diagnosis, it identifies which set of nerves do not work properly. Such conditional is commonly called Radiculopathy. The main tool of pattern diagnosis is the dermatome map as shown in Figure 1. *Pathophysiological diagnosis* refers to the original cause of symptoms where discoligamentous injury is the most common factor in the neuropathic pathophysiological diagnosis.

¹The simulator is available at <https://github.com/TURuibo/Neuropathic-Pain-Diagnosis-Simulator>.

Table 1: Diagnostic records and dataset.

(a) A typical neuropathic pain diagnostic record. "L" and "R" stand for "left" and "right".

Symptom diagnosis: R back thigh discomfort, R knee discomfort, L knee thigh discomfort, Patellofemoral pain syndrome
Pattern diagnosis: L L5 Radiculopathy, R L5 Radiculopathy
Pathophysiological diagnosis: Discoligment injury L4-5

(b) Given many patient records, a diagnostic record dataset takes the following form. "ID" represents different patients. "DLI" and "Radi" stand for discoligamentous injury and radiculopathy. Each row is a patient's diagnostic record in which "1" represents that the patient has the symptom and "0" represents that the patient has no such symptom.

ID	DLI C1-C2	DLI C2-C3	...	L C5 Radi	...	R knee	L neck	...
1	0	0	...	1	...	1	0	...
2	1	0	...	0	...	0	1	...
...
n	0	1	...	0	...	0	0	...

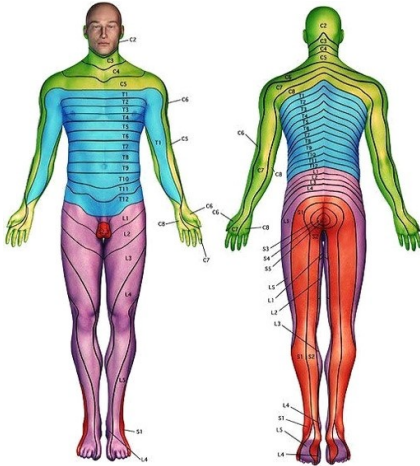


Figure 1: Dermatome map (image source [1]) shows surface regions of different nerves.

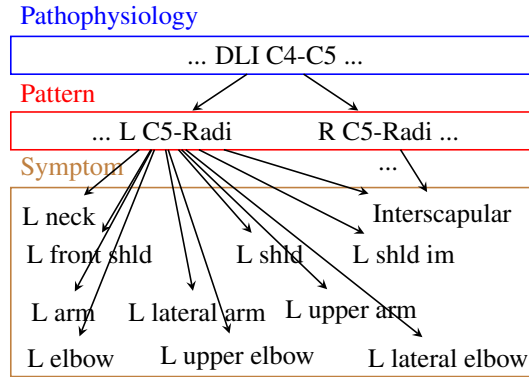


Figure 2: Typical structure of the ground-truth causal graph. "DLI" and "Radi" represent discoligamentous injury and radiculopathy. "shldr" and "im" stand for shoulder and impingement. "L" and "R" stand for left and right. We show the left side symptoms, and the corresponding connections are the same on the right side.

Given a set of patient data, we can present the data as in Table 1b, where 1 indicates that the diagnostic label exists in a patient record and 0 otherwise.

In neuropathic pain diagnoses causal relations are well studied in biomedical research [27, 43]. In general, neuropathic pain symptoms in symptom diagnosis are mainly caused by radiculopathies (Radi) in the pattern diagnosis, and the radiculopathy is mostly caused by discoligamentous injuries (DLI) in the pathophysiological diagnosis. For example, some of the causal relations are shown in Figure 2. DLI C4-C5 causes left side C5 radiculopathy and right side C5 radiculopathy. Left side C5 radiculopathy further causes symptoms at the left front shoulder, the left lateral arm, etc. We see that these locations are consistent with the dermatome map in Figure 1. Despite that there are other causes of neuropathic pain symptoms and radiculopathies such as tumors and diabetes, they rarely appear in primary care. Therefore, we focus on the causal relations among the discoligamentous injuries, radiculopathies, and neuropathic pain symptoms in this work.

The complete causal relations are summarized in Appendix A, and we further provide interactive causal graph visualization at: <https://cutt.ly/BekNFSy>. The causal graph is similar to Figure 2 and consists of three layers: Symptom diagnosis, pattern diagnosis, and pathophysiological diagnosis.

Nodes in each layer have no connection with each other. Arrows either point from nodes in the pathophysiological diagnosis layer to nodes in the pattern diagnosis layer or from nodes in the pattern diagnosis layer to nodes in the symptom diagnosis layer. The causal graph also contains different d-separations such as the fork structure, denoted by \wedge structure (e.g., Left C5 Radiculopathy \leftarrow Discoligamentous injury C4-C5 \rightarrow Right C5 Radiculopathy), the collider structure, denoted by \vee structure (e.g., Left C5 Radiculopathy \rightarrow Left neck pain \leftarrow Left C4 Radiculopathy), and the chain structure (e.g., Discoligamentous injury C4-C5 \rightarrow Left C5 Radiculopathy \rightarrow Left Neck pain).

2.2 Neuropathic Pain Diagnosis Simulator

With the domain knowledge mentioned in Section 2.1, we create our simulator to generate patient diagnostic records.

Real-world diagnostic records. To make our generated records close to the real-world scenario, we learn parameters from a dataset including 141 patient diagnostic records [46]². These patients' diagnostic records are represented as a table of binary variables as shown in Table 1b. The variables in the pathophysiological diagnosis consist of the craniocervical junction injury and 26 discoligamentous injuries; the variables in the pattern diagnosis include 52 radiculopathies; the variables in the symptom diagnosis contain 143 symptoms. Similar to the real-world diagnostic records, the columns of generated records are the mentioned variables and the rows represent the synthetic patients.

Parameter estimation of the causal graph. We estimate the Conditional Probability Distribution (CPD) of each variable given its parents in the causal graph with the real dataset. We compute the CPD of a variable X by $P(X | Pa(X)) = \frac{P(X, Pa(X))}{P(Pa(X))}$, where $Pa(X)$ represents the parents of X in the causal graph. Since variables are binary, the joint distributions can be computed using the number of variable values in the dataset. However, we cannot estimate the CPDs accurately for the variables with many parents because of the curse of dimensionality and the limited number of the real data. Therefore, instead of computing the CPD of X given all its parents, we introduce the heuristic

$$P(X = 1 | Pa(X) = \mathbf{c}) := \max_{i \in I_1} P(X = 1 | Pa_i(X) = c_i), \quad (1)$$

where \mathbf{c} is a given vector of parent values (which can contain either value zero or one), and I_1 is a subset of the index of all variables in $Pa(X)$ such that for $\forall i \in I_1$, $Pa_i(X) \in Pa(X)$ and $c_i = 1$. The condition of Equation 1 is that there exists $c_i \in \mathbf{c}$ such that $c_i = 1$. This condition is satisfied in the real data. Given the parent values \mathbf{c} , we only consider the parents taking the value one, and get the maximum conditional probability of $X = 1$ given a parent taking the value one in \mathbf{c} to estimate the CPD of $P(X = 1 | Pa(X) = \mathbf{c})$.

This approximation is supported by the medical insights. Intuitively, if a symptom is caused by multiple nerves, the chance for the symptom to exist in general is higher when these causes occur at the same time comparing to only one of the causes occurs. For example, both $L4$ and $L5$ radiculopathies can cause knee pain. The chance that a person with both $L4$ and $L5$ radiculopathies feels knee pain is higher or equal to the chance that a person with either one of the radiculopathies feels knee pain. In other words, $P(X = 1 | Pa_1(X) = 1, Pa_2(X) = 1) \geq P(X = 1 | Pa_1(X) = 1)$ and $P(X = 1 | Pa_1(X) = 1, Pa_2(X) = 1) \geq P(X = 1 | Pa_2(X) = 1)$, where $Pa_1(X)$ and $Pa_2(X)$ are $L4$ and $L5$ radiculopathies and X is knee pain.

Given all the conditional probability and marginal probability distributions, we use ancestral sampling to sample neuropathic pain diagnosis data of synthetic patients.

2.3 Simulating Data with Practical Issues of Causal Discovery

Causal discovery is facing many practical issues when applied in real-world applications. Our simulator has many advantages over real datasets in evaluating causal discovery algorithms in the presence of these challenges. In this section, we introduce how to use our simulator to generate

²The dataset is collected in a hospital department specialized in neuropathic pain [46]. Only Ruibo Tu and Bo C. Bertilson get access to the dataset during the course of the project.

datasets exhibiting different open problems. In Section 4 we show experimental results of applying causal discovery algorithms to these simulated data reflecting different real-world problems.

Unmeasured Confounding. Most causal discovery algorithms assume that all variables of concern are observed. However, in most real-life applications collected datasets may not cover all factors to discover causal relations of interest. If there is an unobserved common direct cause of two or more observed variables, this may produce wrong causal conclusions. This problem is known as unmeasured confounding, which is one of the common issues that one is faced with when applying causal discovery algorithms. Addressing unmeasured confounding is an active research direction [18, 20, 28, 40, 47].

There are many ways for our simulator to generate datasets of unmeasured confounding. We can delete the data of parent nodes in a \wedge structure. More specifically, deleting the simulated data of the pathophysiology diagnosis and the pattern diagnosis variables leads to confounding in the dataset because they have at least two direct effects. We can also introduce external variables as confounders in the data generation process. For example, we can add patients' occupation as a confounder which is not included in the given causal graph. The occupation affects daily activities and then increases the risk level of injuring different spine parts. With such datasets, we can evaluate how unmeasured confounding influences the results of causal discovery algorithms and hopefully develop new and better algorithms to address this issue.

Selection bias. Selection bias is an important issue in learning causal structures from real-world observational data. In practice, it is a common scenario where the data collection process is influenced by some attributes of variables. For example, samples in a dataset are not drawn randomly from the population, but from the people who have higher degrees than a bachelor's degree. Then, the selection variable is whether a person has a higher degree than a bachelor's degree. Such selection bias is non-trivial to be removed from the collected dataset and may introduce erroneous causal relations in the results of causal discovery algorithms. Few methods have been developed to address this issue [11, 12, 39, 47, 48]. We can also introduce selection bias to the simulated data. We first choose variables which the selection depends on, and then remove or maintain records based on the values of the chosen variables in the simulated dataset.

Missing data. Missing data is a ubiquitous issue, especially in healthcare. It is common to classify missingness mechanisms into Missing Completely At Random (MCAR), Missing At Random (MAR), and Missing Not At Random (MNAR) [32]. Among them, MAR and MNAR may introduce wrong causal conclusions if one simply deletes the data with missing entries, and applies causal discovery algorithms to the deleted complete dataset. Thus, methods that can handle different missingness mechanisms are much in demand for causal discovery [23, 24, 38, 42, 44].

Using our simulator, we can easily generate data with different missingness mechanisms. We can introduce missingness indicators to our causal graph. We then introduce causal relations between missingness indicators and substantive variables, depending on the missingness mechanism wanted. In the end, we sample the missingness indicators and mask out the data according to the values of missingness indicators.

3 Simulation Quality

We now evaluate whether generated data from our simulator have the similar property to the real-world data. We examine the quality of our simulated data by medical experts and statistical analysis.

3.1 Physician Evaluation

To examine the quality of our simulated data, we mix 50 simulated records with 50 records sampled from the real-world dataset. We then ask a physician specialized in neuropathic pain diagnoses to rate the 100 mixed records with the following score system:

- Score 1: This is not likely to be a real patient (possible but never see such patient before);
- Score 2: This is likely to be a real patient but is not very common (similar cases have happened before but rarely);

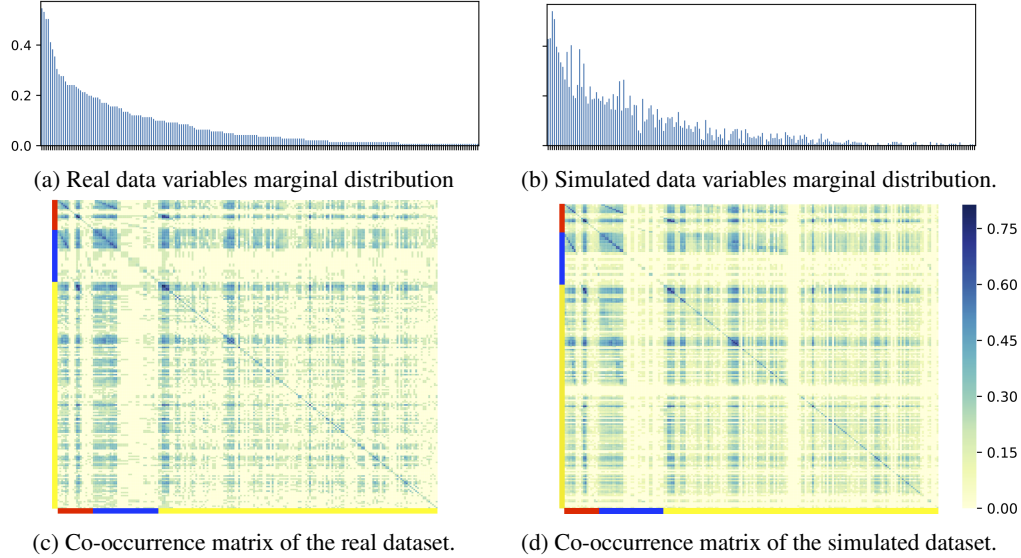


Figure 4: Comparison of the marginal distributions and the co-occurrence matrices of the real and simulated datasets. The orders of variables are the same in Panel (a) and (b). In Panel (c) and (d), the **red color** represents pathophysiological diagnosis, the **blue color** represents pattern diagnosis, and the **yellow color** represents symptom diagnosis.

- Score 3: This is a common patient (similar cases show up time by time);
- Score 4: This is a typical patient (similar cases show up very often).

The physician evaluates the 100 records without knowing the source of the records (the simulator or the real dataset). Figure 3 shows the physician’s evaluation results of the real and the synthetic data. The number of records with higher scores is increasing with the synthetic data which is expected due to our score design. The simulator generates less unlikely diagnostic records than those in the real datasets, which may be due to the missing and noisy labels in the real-world data. Also, when one or two unlikely diagnostic records are generated within many likely diagnostic labels in a record, the physician considers the case as "likely". This case happens more in the simulated data than the real-world data. In general, the result shows that the physician cannot differ the generated data from the real-world data. Also, the simulated data follow the desired frequency (increased numbers for higher scores) from the physician evaluation.

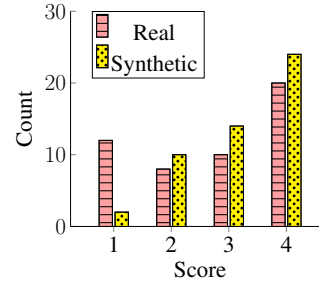


Figure 3: Physician’s evaluation results of 50 real data and 50 simulated data.

3.2 Data Properties

We compare the marginal probability distributions of the same variables in the real dataset and the simulated dataset as shown in Figure 4a and Figure 4b. It shows that marginal probability distributions of variables in both datasets are similar.

We use the co-occurrence matrix normalized by the sample size to show the relation between each pair of variables in Figure 4c and Figure 4d³. For example, the upper left corner of the co-occurrence matrices represents the relations between the variables in the pathophysiological diagnosis and the pattern diagnosis. We find that the pattern of the simulated data is similar to that of the real data. In our simulator, we give no constraints on the relations between both sides of variables, e.g. it is

³For better visualization, we further compute the cubic root of the values in the co-occurrence matrices.

Table 2: Results of causal discovery algorithms using the real dataset and the simulated dataset with the same sample size. "CauAcc" and "Sim" represent "Causal Accuracy" and "Simulated".

	CauAcc				F1		Recall		Precision	
	PC	GES	FCI	RFCI	PC	GES	PC	GES	PC	GES
Real	0.041	0.038	0.024	0.021	0.044	0.037	0.025	0.022	0.187	0.199
Sim	0.038	0.063	0.023	0.016	0.047	0.076	0.025	0.043	0.425	0.377

Table 3: Results of different causal discovery algorithms with different sample sizes. The performance is better when causal accuracy and F1 score have larger values.

Sample size	128	256	512	1024	2048	4096	8192	16384
F1 _{PC}	0.019	0.028	0.016	0.040	0.066	0.100	0.142	0.188
F1 _{GES}	0.042	0.083	0.120	0.150	0.173	0.217	0.261	0.325
CauAcc _{PC}	0.009	0.012	0.009	0.020	0.031	0.048	0.066	0.094
CauAcc _{GES}	0.020	0.045	0.067	0.085	0.105	0.134	0.162	0.230
CauAcc _{RFCI}	0.021	0.023	0.027	0.033	0.036	0.041	0.053	0.070
CauAcc _{FCI}	0.026	0.029	0.034	0.039	0.045	0.051	0.062	0.082

possible to have a connection between left C5 radiculopathy and right neck pain in the graph. We also compare the correlation matrices in Appendix B.

4 Evaluating Causal Discovery Algorithms with Proposed Simulator

We evaluate major causal discovery algorithms with datasets generated from our simulator. We first further evaluate the simulation quality by comparing the causal discovery results on a real-world dataset and a simulated dataset. One advantage of the simulator is that we can generate any amount of data. Thus, we can evaluate causal discovery algorithms with different sample sizes to show the asymptotic property of causal discovery algorithms. Next, we apply causal discovery algorithms to the simulated datasets with different practical issues: Unmeasured confounding, selection bias, and missing data.

We use the causal discovery algorithms implemented by Tetrad [41]. In the experiments the causal discovery algorithms comprise: Constraint-based methods, PC, FCI [40], and RFCI [10]; score-based method, GES [6]. PC and GES output Complete Partially Directed Acyclic Graph (CPDAG), while FCI and RFCI output Partial Ancestral Graph (PAG). We use the F1 score and causal accuracy [7] as the evaluation metrics. Results of other metrics such as Structural Hamming Distance (SHD), precision, and recall are shown in Appendix .

Comparison between simulated and real data. We sample 141 patient records from our simulator with the same sample size as the real-world dataset. We apply causal discovery algorithms to both datasets. Their results are shown in Table 2. We find that the causal accuracies and F1 scores of both datasets are similar and the algorithms in the table cannot recover most edges of the ground-truth causal graph. The reason might be that the real dataset has a small sample size 141 compared with the number of nodes and edges in the causal graph. Moreover, Figure 4a shows that the appearance frequencies of diagnostic labels in the real dataset decay exponentially, which means that many diagnostic labels only appear in few patient diagnostic records. This is especially difficult for these methods because they are based on conditional independence tests that require sufficient samples. Furthermore, we find that the recall rates of PC on both datasets are similar and the precision rate of PC on the simulated dataset is higher than the precision rate on the real dataset. The reason might be that we generate values of a variable only based on the values of its parents. Consequently, our simulator can cancel out the influence of unknown confounders, such as age and occupation of the patient, and other practical issues in the real dataset. We also find that GES benefits relatively more than other methods from such property of the simulated dataset.

Sample size. To show the influence of the sample size, we generate simulated datasets with sample size 128, 256, 512, 1024, 2048, 4096, 8192, and 16384. Under certain assumptions, these methods are asymptotically correct when infinite data are available. Table 3 shows that the performance of the algorithms is improved with increasing the sample size, when there is no selection bias,

unknown confounders, or missing values. However, all these methods are not sample efficient as the performance is still low and has not saturated even with 16834 data points. Thus, developing sample efficient causal discovery algorithms is needed, especially when real-life data are costly.

Confounding. We generate simulated data with external variables as confounders (see Appendix C for details). We compare the performance of FCI and RFCI on the dataset containing unknown confounders with that without confounders. The sample size of both datasets is 1024. The causal accuracy is 0.033 and 0.030 on the dataset with unknown confounders, and 0.039 and 0.033 on the dataset without unknown confounders. The results of the FCI algorithms on the dataset with unknown confounders are slightly worse than that without unknown confounders because the FCI algorithms consider the unknown confounders and output Partial Ancestral Graph (PAG) that provides the information about potential unknown confounders. However, it is far from ideal. We also generate confounding data by deleting all the data of the common parents in the causal graph. The results are shown in Appendix C.

Selection bias. We choose both sides of $C6$, $C7$, $L5$, and $S1$ radiculopathy as the causes of a selection variable. We then delete the simulated data regarding the values of the selection variable. We interpret this setting as a situation where the patients without those radiculopathies hardly ever go to the hospital; thus, the hospital hardly collects their data. Table 4 shows the results on the dataset with selection bias and the reference one without selection bias. RFCI is more robust to selection bias than FCI, even both should be able to handle it by design. For the algorithms without considering selection bias, the causal accuracy of GES outperforms PC.

Table 4: Results of different causal discovery methods in the presence of selection bias.

	FCI	RFCI	PC	GES
CauAcc	0.039	0.039	0.031	0.109
CauAcc _{ref}	0.046	0.037	0.033	0.114

Missing data. We evaluated the performance on all three missingness mechanisms: MCAR, MAR, and MNAR. We generate missing values in the dataset according to the definition in [23]. To generate the data that are MCAR, the probability distribution of missing values follows the Bernoulli distribution with the missingness probability 0.0007. To generate the data that are MAR, we choose variables in the pattern diagnosis as the causes of missingness indicators and variables in the pathophysiological diagnosis and the symptom diagnosis as the variables with missing values. Likewise, to generate the data that are MNAR, the variables with missing values are chosen in the range of all the variables in the causal graph. Since FCI, PC, and GES cannot deal with the dataset containing missing values, we delete the records containing any missing value and input the deleted complete dataset. The sample size of the deleted complete dataset is 7042. As a reference, we create a simulated dataset whose sample size is 7042 without missing values.

Table 5 shows that the results of MAR and MNAR experiments are worse than the results of MCAR experiments, which are close to the reference one without missing values. This is expected as [44] shows: When the data are MCAR, causal discovery results are asymptotically correct; when the data are MAR and MNAR, these algorithms may produce erroneous edges in the case where the missingness indicators are the common children or descendants of the common children of the concerned variables. We then check the number of missingness indicators satisfying this conclusion. It is 4 in MNAR and 7 in MAR out of total 52 missingness indicators.

Table 5: Results of applying causal discovery algorithms to the MCAR, MAR, and MNAR datasets.

	FCI	RFCI	PC	GES
CauAcc _{MNAR}	0.059	0.051	0.061	0.154
CauAcc _{MAR}	0.063	0.049	0.050	0.135
CauAcc _{MCAR}	0.066	0.055	0.067	0.161
CauAcc _{ref}	0.062	0.050	0.059	0.145
F1 _{MNAR}	X	X	0.133	0.251
F1 _{MAR}	X	X	0.132	0.241
F1 _{MCAR}	X	X	0.141	0.256
F1 _{ref}	X	X	0.156	0.253

5 Related Work

The evaluation of causal discovery algorithms mainly consists of synthetic and real data experiments. Synthetic data are mostly sampled from randomly generated graph structures, or based on models

proposed in different works. Such synthetic data experiments can show the superior performance of proposed methods but sometimes may oversimplify the challenges in real-world scenarios [15]. Unfortunately, there are few available real-world datasets for evaluating causal discovery algorithms. Mooij et al. [25] provided a set of cause-effect pairs with ground-truth causal relations. However, the cause-effect pairs can be used for a limited range of causal discovery methods such as the Linear Non-Gaussian Acyclic Model (LiNGAM) [37]. Also, the dataset containing only pair-wise data is not complex enough to evaluate causal discovery algorithms in real-world scenarios. Several other datasets from genomics [30, 35, 14] and health-care [44] contain causal relations among multiple variables and are commonly used for the evaluation; however, few pairs of ground-truth causal relations are known/labeled by domain experts and the evaluation is not systematic. Therefore, it is necessary to develop causal discovery benchmarks for real-world evaluation.

Filling the gap between the synthetic and real data evaluation [17], the simulator in the context of real-world applications is needed. Glymour et al. [17] discussed the evaluation of search tasks, especially causal discovery, and concluded that simulation is a desired way to evaluate the research in this direction. Despite the argument, [17] did not build any simulator instance. Very recently, a few simulators for causal discovery evaluation have been developed, especially considering time-series data. Sanchez-Romero et al. [36] generated simulated fMRI data over time with the focus on the situation where feedback loops exist. Runge et al. [33] provided ground-truth time-series datasets by mimicking properties of real climate and weather datasets. However, these simulators are still limited to the complexity reflecting real-world causal discovery demands and are not suitable for evaluating the causal discovery methods for static data.

In machine learning, there are many simulators built for other disciplines. For example, reinforcement learning benefits from the simulators covering practical issues with different applications [8, 5, 19]. Some of them are used for evaluating sequential decision making by considering counterfactual outcomes. Oberst and Sontag [26] simulated data about treating sepsis among intensive care unit (ICU) patients. The data consist of vital signs, treatment options, and the final mortality with a fully specified underlying Markov Decision Process. Another simulator [16] is used for evaluating the performance of the treatment response over time [21]. Geng et al. [16] provided the dynamics of the tumor volume and its relation with chemotherapy, tumor growth, and radiation. Given parameters of the dynamic equations, Lim [21] simulated the data satisfying this domain knowledge and introduced the practical issues such as unmeasured confounding. However, these simulators contribute to advancing the research on estimating treatment response over time but not causal discovery.

6 Discussion

In this work, we build a simulator in the neuropathic pain diagnosis setting for evaluating causal discovery algorithms. Our simulator is based on ground-truth causal relations regarding the domain knowledge, and its parameters are estimated with a real-world dataset. It contains 222 nodes and 770 edges establishing complex real-world challenges. Our simulator can generate any amount of synthetic records that are indistinguishable from real-world records judged by physicians. The simulator can also simulate practical issues in causal discovery research such as missing data, selection bias, and unknown confounding. We demonstrated how to evaluate causal discovery algorithms using our simulator for different challenges.

Our simulator not only contributes to causal discovery research but also machine learning in healthcare research where public data are extremely scarce due to privacy concerns. In the future, we will refine our simulator to consider border scenarios. At the same time, we will seek further opportunities to build different simulators for causal discovery evaluation and machine learning in healthcare research.

Acknowledgements. Kun Zhang would like to acknowledge the support by National Institutes of Health under Contract No. NIH-1R01EB022858-01, FAIR01EB022858, NIH-1R01LM012087, NIH-5U54HG008540-02, and FAIR- U54HG008540, by the United States Air Force under Contract No. FA8650-17-C-7715, and by National Science Foundation EAGER Grant No. IIS-1829681. The National Institutes of Health, the U.S. Air Force, and the National Science Foundation are not responsible for the views reported in this article.

In addition, the authors thank Akshaya Thippur Sridatta and Tino Weinkauff for the help of the audio dubbing of the 3-minute introduction video and the visualization of the causal graph.

References

- [1] Dermatone map source. <https://i.pining.com/736x/ef/76/47/ef7647ceae98d10588f14b4ecd7e6a89.jpg>.
- [2] D. Amodei, S. Ananthanarayanan, R. Anubhai, J. Bai, E. Battenberg, C. Case, J. Casper, B. Catanzaro, Q. Cheng, G. Chen, et al. Deep speech 2: End-to-end speech recognition in english and mandarin. In *International conference on machine learning*, pages 173–182, 2016.
- [3] E. Bareinboim, I. Guyon, D. Blei, N. Meinshausen, C. Szepesvári, S. Magliacane, and Y. Bengio. Panel discussion on datasets and benchmarks for causal learning. <https://www.youtube.com/watch?v=QaoijubZTTA>, 2008.
- [4] A. Bewley, J. Rigley, Y. Liu, J. Hawke, R. Shen, V.-D. Lam, and A. Kendall. Learning to drive from simulation without real world labels. *arXiv preprint arXiv:1812.03823*, 2018.
- [5] G. Brockman, V. Cheung, L. Pettersson, J. Schneider, J. Schulman, J. Tang, and W. Zaremba. Openai gym. *arXiv preprint arXiv:1606.01540*, 2016.
- [6] D. M. Chickering. Optimal structure identification with greedy search. *Journal of machine learning research*, 3(Nov):507–554, 2002.
- [7] T. Claassen and T. Heskes. A bayesian approach to constraint based causal inference. *arXiv preprint arXiv:1210.4866*, 2012.
- [8] K. Cobbe, O. Klimov, C. Hesse, T. Kim, and J. Schulman. Quantifying generalization in reinforcement learning. *arXiv preprint arXiv:1812.02341*, 2018.
- [9] L. Colloca, T. Ludman, D. Bouhassira, R. Baron, A. H. Dickenson, D. Yarnitsky, R. Freeman, A. Truini, N. Attal, N. B. Finnerup, et al. Neuropathic pain. *Nature reviews Disease primers*, 3: 17002, 2017.
- [10] D. Colombo, M. H. Maathuis, M. Kalisch, and T. S. Richardson. Learning high-dimensional directed acyclic graphs with latent and selection variables. *The Annals of Statistics*, pages 294–321, 2012.
- [11] J. D. Correa and E. Bareinboim. Causal effect identification by adjustment under confounding and selection biases. In *Thirty-First AAAI Conference on Artificial Intelligence*, 2017.
- [12] C. Cortes, M. Mohri, M. Riley, and A. Rostamizadeh. Sample selection bias correction theory. In *International conference on algorithmic learning theory*, pages 38–53. Springer, 2008.
- [13] J. Deng, W. Dong, R. Socher, L.-J. Li, K. Li, and L. Fei-Fei. Imagenet: A large-scale hierarchical image database. In *2009 IEEE conference on computer vision and pattern recognition*, pages 248–255. Ieee, 2009.
- [14] A. Dixit, O. Parnas, B. Li, J. Chen, C. P. Fulco, L. Jerby-Arnon, N. D. Marjanovic, D. Dionne, T. Burks, R. Raychowdhury, et al. Perturb-seq: dissecting molecular circuits with scalable single-cell rna profiling of pooled genetic screens. *Cell*, 167(7):1853–1866, 2016.
- [15] D. Garant and D. Jensen. Evaluating causal models by comparing interventional distributions. *arXiv preprint arXiv:1608.04698*, 2016.
- [16] C. Geng, H. Paganetti, and C. Grassberger. Prediction of treatment response for combined chemo-and radiation therapy for non-small cell lung cancer patients using a bio-mathematical model. *Scientific reports*, 7(1):13542, 2017.
- [17] C. Glymour, J. D. Ramsey, and K. Zhang. The evaluation of discovery: Models, simulation and search through “big data”. *Open Philosophy*, 2(1):39–48, 2019.
- [18] P. O. Hoyer, S. Shimizu, A. J. Kerminen, and M. Palviainen. Estimation of causal effects using linear non-gaussian causal models with hidden variables. *International Journal of Approximate Reasoning*, 49(2):362–378, 2008.

- [19] M. Johnson, K. Hofmann, T. Hutton, and D. Bignell. The malmo platform for artificial intelligence experimentation. In *IJCAI*, pages 4246–4247, 2016.
- [20] N. Kallus, X. Mao, and A. Zhou. Interval estimation of individual-level causal effects under unobserved confounding. In K. Chaudhuri and M. Sugiyama, editors, *Proceedings of Machine Learning Research*, volume 89 of *Proceedings of Machine Learning Research*, pages 2281–2290. PMLR, 16–18 Apr 2019. URL <http://proceedings.mlr.press/v89/kallus19a.html>.
- [21] B. Lim. Forecasting treatment responses over time using recurrent marginal structural networks. In *Advances in Neural Information Processing Systems*, pages 7483–7493, 2018.
- [22] T.-Y. Lin, M. Maire, S. Belongie, J. Hays, P. Perona, D. Ramanan, P. Dollár, and C. L. Zitnick. Microsoft coco: Common objects in context. In *European conference on computer vision*, pages 740–755. Springer, 2014.
- [23] K. Mohan, J. Pearl, and J. Tian. Graphical models for inference with missing data. In *Advances in neural information processing systems*, pages 1277–1285, 2013.
- [24] K. Mohan, F. Thoemmes, and J. Pearl. Estimation with incomplete data: The linear case. In *Proceedings of the Twenty-Seventh International Joint Conference on Artificial Intelligence, IJCAI-18*, pages 5082–5088. International Joint Conferences on Artificial Intelligence Organization, 7 2018. doi: 10.24963/ijcai.2018/705. URL <https://doi.org/10.24963/ijcai.2018/705>.
- [25] J. M. Mooij, J. Peters, D. Janzing, J. Zscheischler, and B. Schölkopf. Distinguishing cause from effect using observational data: methods and benchmarks. *The Journal of Machine Learning Research*, 17(1):1103–1204, 2016.
- [26] M. Oberst and D. Sontag. Counterfactual off-policy evaluation with gumbel-max structural causal models. In *International Conference on Machine Learning*, pages 4881–4890, 2019.
- [27] D. D. Ohnmeiss, H. Vanharanta, and J. Ekholm. Relation between pain location and disc pathology: a study of pain drawings and ct/discography. *The Clinical journal of pain*, 15(3): 210–217, 1999.
- [28] M. Osama, D. Zachariah, and T. Schön. Inferring heterogeneous causal effects in presence of spatial confounding. *arXiv preprint arXiv:1901.09919*, 2019.
- [29] J. Pearl. *Causality*. Cambridge university press, 2009.
- [30] J. Peters, P. Bühlmann, N. Meinshausen, et al. Causal inference by using invariant prediction: identification and confidence intervals. *Journal of the Royal Statistical Society Series B*, 78(5): 947–1012, 2016.
- [31] J. Peters, D. Janzing, and B. Schölkopf. *Elements of causal inference: foundations and learning algorithms*. MIT press, 2017.
- [32] D. B. Rubin. Inference and missing data. *Biometrika*, 63(3):581–592, 1976.
- [33] J. Runge, S. Bathiany, E. Bollt, G. Camps-Valls, D. Coumou, E. Deyle, C. Glymour, M. Kretschmer, M. D. Mahecha, J. Muñoz-Marí, et al. Inferring causation from time series in earth system sciences. *Nature communications*, 10(1):2553, 2019.
- [34] O. Russakovsky, J. Deng, H. Su, J. Krause, S. Satheesh, S. Ma, Z. Huang, A. Karpathy, A. Khosla, M. Bernstein, et al. Imagenet large scale visual recognition challenge. *International journal of computer vision*, 115(3):211–252, 2015.
- [35] K. Sachs, O. Perez, D. Pe’er, D. A. Lauffenburger, and G. P. Nolan. Causal protein-signaling networks derived from multiparameter single-cell data. *Science*, 308(5721):523–529, 2005.
- [36] R. Sanchez-Romero, J. D. Ramsey, K. Zhang, M. R. Glymour, B. Huang, and C. Glymour. Estimating feedforward and feedback effective connections from fmri time series: Assessments of statistical methods. *Network Neuroscience*, 3(2):274–306, 2019.
- [37] S. Shimizu, P. O. Hoyer, A. Hyvärinen, and A. Kerminen. A linear non-gaussian acyclic model for causal discovery. *Journal of Machine Learning Research*, 7(Oct):2003–2030, 2006.

- [38] I. Shpitser. Consistent estimation of functions of data missing non-monotonically and not at random. In *Advances in Neural Information Processing Systems*, pages 3144–3152, 2016.
- [39] P. Spirtes, C. Meek, and T. Richardson. Causal inference in the presence of latent variables and selection bias. In *Proceedings of the Eleventh conference on Uncertainty in artificial intelligence*, pages 499–506. Morgan Kaufmann Publishers Inc., 1995.
- [40] P. Spirtes, C. N. Glymour, R. Scheines, D. Heckerman, C. Meek, G. Cooper, and T. Richardson. *Causation, prediction, and search*. 2000.
- [41] P. Spirtes, C. Glymour, and R. Scheines. The tetrad project: Causal models and statistical data. pittsburgh, 2004.
- [42] E. V. Strobl, S. Visweswaran, and P. L. Spirtes. Fast causal inference with non-random missingness by test-wise deletion. *International Journal of Data Science and Analytics*, pages 1–16.
- [43] Y. Tanaka, S. Kokubun, T. Sato, and H. Ozawa. Cervical roots as origin of pain in the neck or scapular regions. *Spine*, 31(17):E568–E573, 2006.
- [44] R. Tu, C. Zhang, P. Ackermann, K. Mohan, H. Kjellström, and K. Zhang. Causal discovery in the presence of missing data. In K. Chaudhuri and M. Sugiyama, editors, *Proceedings of Machine Learning Research*, volume 89 of *Proceedings of Machine Learning Research*, pages 1762–1770. PMLR, 16–18 Apr 2019. URL <http://proceedings.mlr.press/v89/tu19a.html>.
- [45] F. Wang, M. Jiang, C. Qian, S. Yang, C. Li, H. Zhang, X. Wang, and X. Tang. Residual attention network for image classification. In *Proceedings of the IEEE Conference on Computer Vision and Pattern Recognition*, pages 3156–3164, 2017.
- [46] C. Zhang, H. Kjellstrom, C. H. Ek, and B. C. Bertilson. Diagnostic prediction using discomfort drawings with IBTM. In *MLHC*, 2016.
- [47] J. Zhang. On the completeness of orientation rules for causal discovery in the presence of latent confounders and selection bias. *Artificial Intelligence*, 172(16-17):1873–1896, 2008.
- [48] K. Zhang, J. Zhang, B. Huang, B. Schölkopf, and C. Glymour. On the identifiability and estimation of functional causal models in the presence of outcome-dependent selection. In *UAI*, 2016.
- [49] K. Zhang, B. Schölkopf, P. Spirtes, and C. Glymour. Learning causality and causality-related learning: some recent progress. *National science review*, 5(1):26–29, 2017.

A Ground-truth Causal Relations

In this paper, we focus on the neuropathic pain caused by discoligamentous injuries and radiculopathies. Table 11 shows all the ground-truth causal relations which are used for establishing the ground-truth causal graph for our simulator. Figure 5 shows the whole causal graph of neuropathic pain diagnose.

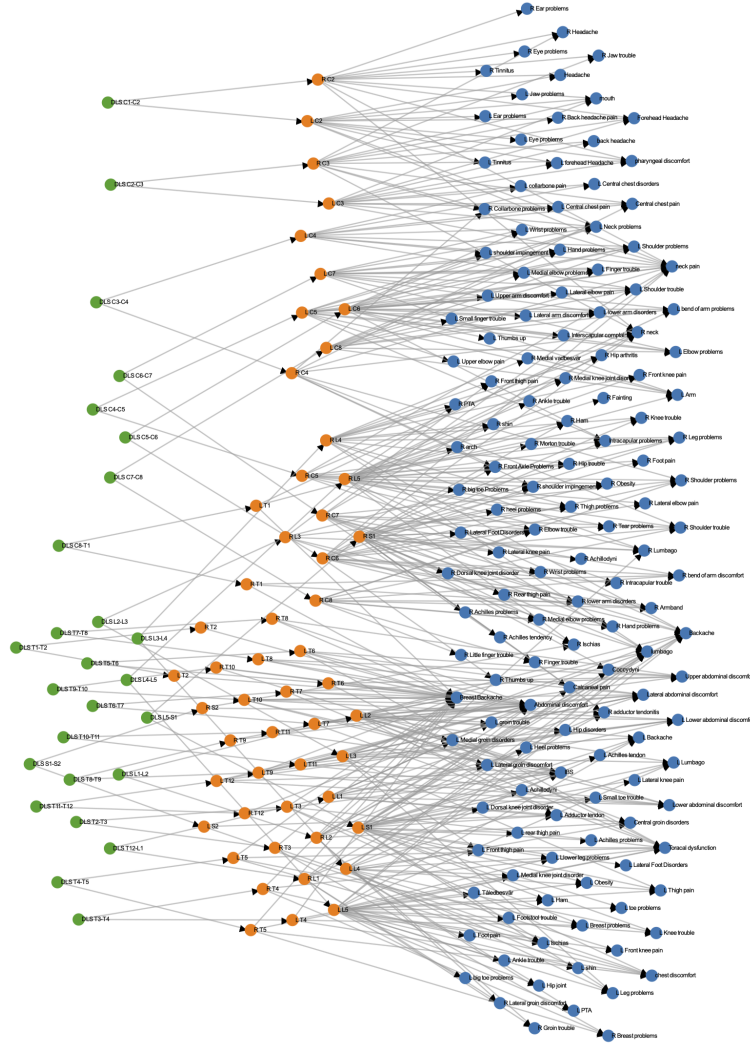


Figure 5: The causal graph of neuropathic pain diagnoses.

B Simulation Quality Evaluation

We show several simulated patient diagnostic records and the corresponding physician’s evaluation scores in Table 6. Moreover, we show the correlation matrices of the real dataset and the simulated dataset in Figure 6. We can clearly see the pattern of the correlation matrix of the simulated dataset, which is similar to the pattern of the correlation matrix of the real dataset. The correlation matrix of the simulated dataset contains many white lines. When all values of a variable are zero in the simulated dataset, the row and the column of the variable in the correlation matrix are white lines. Since our simulator cancels out many correlations between variables which might be introduced by unknown confounders and selection bias, the simulated dataset with a small sample size might have many variables with only zero value. The number of full-zero variables can be controlled by introducing different levels of random noise in the data generation process.

Table 6: A part of the physician’s evaluation results.

Pathophysiology diagnosis	Pattern diagnosis	Symptom diagnosis	Score
DLI L3-L4, DLI T11-T12	L L4 Radiculopathy, R L4 Radiculopathy	L Front thigh pain, R Front thigh pain, R shin	4
DLI C3-C4, DLI L4-L5, DLI L5-S1	L C4 Radiculopathy , R C4 Radiculopathy, L L5 Radiculopathy, R L5 Radiculopathy, L S1 Radiculopathy, R S1 Radiculopathy	L Neck problems, R neck, L collarbone pain, R Front Axle Problems, L shoulder impingement, L Shoulder trouble, R Shoulder problems, R Shoulder trouble, L PTA, L Front knee pain, R Front knee pain, R arch, L Obesity, R Ham, R Tear problems, R heel problems, L Heel problems, L rear thigh pain	4
DLI C2-C3	L C3 Radiculopathy, R C3 Radiculopathy	L Neck problems, R neck	3
DLI C1-C2, DLI C5-C6, DLI C6-C7, DLI S1-S2	L C2 Radiculopathy, R C2 Radiculopathy, L C6 Radiculopathy, R C6 Radiculopathy’, L C7 Radiculopathy, R C7 Radiculopathy	neck pain, L Eye problems, R Eye problems, L Jaw problems, L forehead Headache, R Jaw trouble, L Shoulder problems, R Shoulder problems, L Thumbs up, L Hand problems, R Armband, L Medial elbow problems, R Medial elbow problems	3
DLI L4-L5, DLI L5-S1	L L5 Radiculopathy, R L5 Radiculopathy, L S1 Radiculopathy, R S1 Radiculopathy	R adductor tendonitis , lumbago, R Lumbago, L Hip joint, R Hip arthritis, L Medial knee joint disorder, R shin, R Knee trouble, R Tear problems, L Lateral Foot Disorders, L Heel problems, R Achilles tendency	2
DLI L4-L5, DLI L5-S1	L L5 Radiculopathy, R L5 Radiculopathy, R S1 Radiculopathy	lumbago, L Hip joint, L Ankle trouble, L Footstool trouble, R Dorsal knee joint disorder, Coccydyni, R Rear thigh pain, R Achilles tendency	2

C Experiment Details

In this section, we mainly show recall, precision, and SHD results of causal discovery algorithms under different experiment settings. Table 7, Table 8, Table 9, and Table 10 are the results of the experiments designed for evaluating causal discovery algorithms in the presence of different sample sizes, unknown confounders, selection bias, and missing data.

For generating the datasets with confounders that are external variables, we choose the discoligamentous injury C2-C3, C3-C4, C4-C5, C5-C6, C6-C7, and C7-C8 as the direct effects of an unknown confounder. In this experiment, the confounder can be interpreted as the occupation that can easily damage the neck part of people during the work time. Thus, the chosen discoligamentous injuries are correlated with each other. Then, we use Bernoulli distribution as the marginal distribution of the confounder, and assign a default CPD to each chosen discoligamentous injury. In the end, we generate the data from our modified simulator and delete the data of the introduced confounder in the simulated dataset.

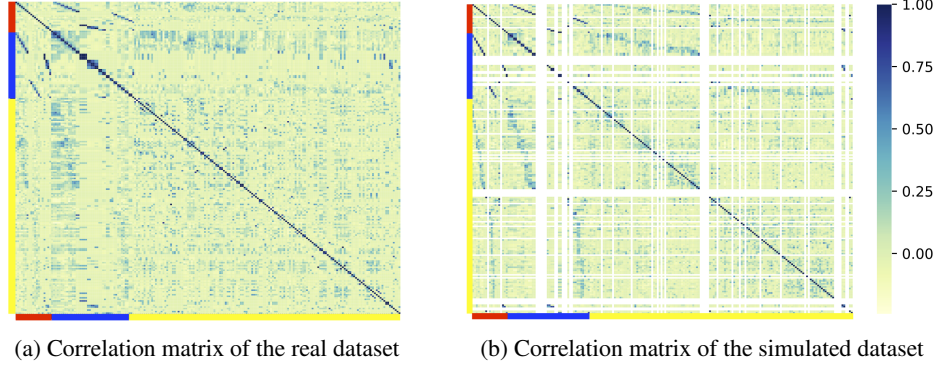


Figure 6: Comparison of the correlation matrices of the real and simulated datasets.

Table 7: Performance of different causal discovery algorithms on the datasets with different sample sizes. The SHD performance is better when it has smaller value. Precision, recall, causal accuracy and F1 score are better when they have larger value. Total SHD is 24642.

Sample size	128	256	512	1024	2048	4096	8192	16384
SHD _{PC}	794.5	809.0	830.0	834.5	826.5	822.5	801.5	802
SHD _{GES}	800.5	802.5	814.0	815.0	824.0	834.0	808.5	773
Precision _{PC}	0.143	0.141	0.069	0.138	0.221	0.301	0.413	0.438
Precision _{GES}	0.200	0.316	0.344	0.361	0.366	0.393	0.441	0.505
Recall _{PC}	0.010	0.0156	0.009	0.023	0.039	0.060	0.086	0.120
Recall _{GES}	0.023	0.048	0.073	0.095	0.113	0.149	0.185	0.239

Table 8: Performance of causal discovery methods in the presence of unknown confounders. Total SHD is 10082. The sample size is 1024.

	FCI	RFCI	GFCI	PC	GES
Cau_Acc	0.013	0.014	0.009	X	X
SHD	X	X	X	123.5	83.5

Table 11: Ground-truth causal relations. A capital letter with a number represents a radiculopathy. For example, "C2" represents "C2 radiculopathy". A radiculopathy as an effect in the table represents both sides of a radiculopathy. A radiculopathy as a cause in the table has the same side with its effect. We denote left as "L" and right as "R".

Effect	Cause
C2	DLS C1-C2
C3	DLS C2-C3
C4	DLS C3-C4
C5	DLS C4-C5
C6	DLS C5-C6
C7	DLS C6-C7
C8	DLS C7-C8
T1	DLS C8-T1
T2	DLS T1-T2
T3	DLS T2-T3
T4	DLS T3-T4
T5	DLS T4-T5
T6	DLS T5-T6
T7	DLS T6-T7
T8	DLS T7-T8
T9	DLS T8-T9
T10	DLS T9-T10
T11	DLS T10-T11

T12	DLS T11-T12
L1	DLS T12-L1
L2	DLS L1-L2
L3	DLS L2-L3
L4	DLS L3-L4
L5	DLS L4-L5
S1	DLS L5-S1
S2	DLS S1-S2
C2	craniocervical junction
C3	craniocervical junction
C4	craniocervical junction
Ibs	T10;T11;T12;L1;L2
L neck problems	C2;C3;C4;C5;C6;C7
Neck pain	C2;C3;C4;C5;C6;C7
R neck	C2;C3;C4;C5;C6;C7
L tinnitus	C2
L eye problems	C2
L ear problems	C2
R tinnitus	C2
R eye problems	C2
R ear problems	C2
Headache	C2
L jaw problems	C2
L forehead headache	C2;C3
Mouth	C2;C3
Forehead headache	C2;C3
R headache	C2;C3
R pta	L4;L5
Pharyngeal discomfort	C2;C3
R jaw trouble	C2;C3
Back headache	C3
R back headache pain	C3
L collarbone pain	C3;C4
R collarbone problems	C3;C4
Central chest pain	C3;C4
L central chest pain	C3;C4
L central chest disorders	C3;C4
R front axle problems	C4;C5;C6
L shoulder impingement	C4;C5;C6
R shoulder impingement	C4;C5;C6
L shoulder problems	C4;C5;C6;C7;C8
L shoulder trouble	C4;C5;C6;C7;C8
R shoulder problems	C4;C5;C6;C7;C8
R shoulder trouble	C4;C5;C6;C7;C8
L upper arm discomfort	C5
L upper elbow pain	C5
Intracapular problems	C5;C6
L interscapular complaints	C5;C6
R intracapular trouble	C5;C6
L lateral elbow pain	C5;C6
L lateral arm discomfort	C5;C6
R lateral elbow pain	C5;C6
L elbow problems	C5;C6;C7;C8
R elbow trouble	C5;C6;C7;C8
L arm	C5;C6;C7;C8;T1
L thumbs up	C6
R thumbs up	C6
L wrist problems	C6;C7
R wrist problems	C6;C7

L lower arm disorders	C6;C7;C8
R lower arm disorders	C6;C7;C8
L hand problems	C6;C7;C8
R hand problems	C6;C7;C8
L bend of arm problems	C6;C7;C8;T1
R armband	C6;C7;C8;T1
R bend of arm discomfort	C6;C7;C8;T1
L medial elbow problems	C7;C8
R medial elbow problems	C7;C8
L finger trouble	C7;C8
R finger trouble	C7;C8
L small finger trouble	C8
R little finger trouble	C8
L groin trouble	L1;L2
L medial groin disorders	L1;L2
L lateral groin discomfort	L1;L2
Central groin disorders	L1;L2
R lateral groin discomfort	L1;L2
R groin trouble	L1;L2
L adductor tendon	L1;L2;S1;S2
R adductor tendonitis	L1;L2;S1;S2
L hip disorders	L2;L3
L backache	L2;L3;L4;L5;S1
Backache	L2;L3;L4;L5;S1
L lumbago	L2;L3;L4;L5;S1
Lumbago	L2;L3;L4;L5;S1
R lumbago	L2;L3;L4;L5;S1
L front thigh pain	L3;L4
R front thigh pain	L3;L4
R thigh problems	L3;L4;L5;S1
L leg problems	L3;L4;L5;S1
L thigh pain	L3;L4;L5;S1
R leg problems	L3;L4;L5;S1
R medial vadbesvär	L4
L pta	L4;L5
L hip joint	L4;L5
R hip trouble	L4;L5
R hip arthritis	L4;L5
L medial knee joint disorder	L4;L5
L front knee pain	L4;L5
R medial knee joint disorder	L4;L5
R front knee pain	L4;L5
L shin	L4;L5
R shin	L4;L5
L llower leg problems	L4;L5;S1
L knee trouble	L4;L5;S1
R knee trouble	L4;L5;S1
L tåledbesvär	L5
L big toe problems	L5
R big toe problems	L5
L foot pain	L5
L ankle trouble	L5
R ankle trouble	L5
L footstool trouble	L5
R arch	L5
R morton trouble	L5
R fainting	L5
L ischias	L5;S1;S2
R ischias	L5;S1;S2

L ham	L5;S1
L obesity	L5;S1
R ham	L5;S1
L toe problems	L5;S1
R foot pain	L5;S1
R tear problems	L5;S1
R obesity	L5;S1
R dorsal knee joint disorder	S1
L dorsal knee joint disorder	S1
L lateral knee pain	S1
R lateral knee pain	S1
L small toe trouble	S1
L lateral foot disorders	S1
R lateral foot disorders	S1
R heel problems	S1
Calcaneal pain	S1
L heel problems	S1
Coccydyni	S1
L rear thigh pain	S1
R rear thigh pain	S1
L achilles problems	S1
L achilles tendon	S1
L achillodini	S1
R achilles problems	S1
R achilles tendency	S1
R achillodini	S1
Breast backache	T1;T2;T3;T4;T5;T6;T7;T8;T9;T10
Chest discomfort	T3;T4;T5
L breast problems	T3;T4;T5
R breast problems	T3;T4;T5
Toracal dysfunction	T3;T4;T5;T6;T7
Upper abdominal discomfort	T6;T7;T8
Lateral abdominal discomfort	T6;T7;T8;T9;T10;T11;T12;L1;L2
Abdominal discomfort	T6;T7;T8;T9;T10;T11;T12;L1;L2
L lower abdominal discomfort	T9;T10;T11;T12;L1;L2
Lower abdominal discomfort	T9;T10;T11;T12;L1;L2

Table 9: Performance of different causal discovery methods in the presence of selection bias.

	F1	F1 ref	Recall	Recall ref	Precision	Precision ref
PC	0.072	0.076	0.042	0.045	0.276	0.236
GES	0.193	0.185	0.126	0.125	0.416	0.356

Table 10: Performance of causal discovery methods in the presence of missing data.

	FCI	RFCI	PC	GES
CauAcc _{MNAR}	0.059	0.051	0.061	0.154
CauAcc _{MAR}	0.063	0.049	0.050	0.135
CauAcc _{MCAR}	0.066	0.055	0.067	0.161
CauAcc _{ref}	0.062	0.050	0.059	0.145
SHD _{MNAR}	X	X	806.5	812.0
SHD _{MAR}	X	X	806.5	778.5
SHD _{MCAR}	X	X	804.5	801.5
SHD _{ref}	X	X	795.0	765.5
Recall _{MNAR}	X	X	0.081	0.177
Recall _{MAR}	X	X	0.080	0.160
Recall _{MCAR}	X	X	0.086	0.181
Recall _{ref}	X	X	0.094	0.168
Precision _{MNAR}	X	X	0.376	0.435
Precision _{MAR}	X	X	0.389	0.490
Precision _{MCAR}	X	X	0.405	0.440
Precision _{ref}	X	X	0.462	0.514
F1 _{MNAR}	X	X	0.133	0.251
F1 _{MAR}	X	X	0.132	0.241
F1 _{MCAR}	X	X	0.141	0.256
F1 _{ref}	X	X	0.156	0.253